AD 749864

AFCRL-72-0404
30 JUNE 1972
PHYSICAL SCIENCES RESEARCH PAPERS, NO. 500

AIR FORCE CAMBRIDGE RESEARCH LABORATORIES

L. G. HANSCOM FIELD, BEDFORD, MASSACHUSETTS

Some Aspects of Optical Evaluation of CO_2 Laser Window Materials at AFCRL

B. BENDOW
A. HORDVIK
H. LIPSON
L. SKOLNIK

D D C
RECEIVED
OCT 16 1972
C

Approved for public release; distribution unlimited.

AIR FORCE SYSTEMS COMMAND
United States Air Force

NATIONAL TECHNICAL
INFORMATION SERVICE

ACCESSION for
NTIS White Section ☑
DDC Buff Section ☐
UNANNOUNCED ☐
JUSTIFICATION.....
.....
BY.....
DISTRIBUTION/AVAILABILITY CODES
Dist. AVAIL. and/or SPECIAL
A

Qualified requestors may obtain additional copies from the Defense Documentation Center.

Unclassified
Security Classification

DOCUMENT CONTROL DATA - R&D

(Security classification of title, body of abstract and indexing annotation must be entered when the overall report is classified)

1. ORIGINATING ACTIVITY *(Corporate author)*
Air Force Cambridge Research Laboratories (LQO)
L. G. Hanscom Field
Bedford, Massachusetts 01730

2a. REPORT SECURITY CLASSIFICATION
Unclassified

2b. GROUP

3. REPORT TITLE
SOME ASPECTS OF THE OPTICAL EVALUATION OF CO_2 LASER WINDOW MATERIALS AT AFCRL

4. DESCRIPTIVE NOTES *(Type of report and inclusive dates)*
Scientific.

5. AUTHOR(S) *(First name, middle initial, last name)*
Bernard Bendow, Herbert G. Lipson
Audun Hordvik, Lyn Skolnik

6. REPORT DATE
30 June 1972

7a. TOTAL NO. OF PAGES
31

7b. NO. OF REFS
10

8a. CONTRACT OR GRANT NO.

b. PROJECT, TASK, WORK UNIT NOS. 5621-08-03

c. DOD ELEMENT 61102F

d. DOD SUBELEMENT 681301

9a. ORIGINATOR'S REPORT NUMBER(S)
AFCRL-72-0404

9b. OTHER REPORT NO(S) *(Any other numbers that may be assigned this report)*
PSRP No. 500

10. DISTRIBUTION STATEMENT
Approved for public release; distribution unlimited.

11. SUPPLEMENTARY NOTES
Presented at the Fifth DoD Conference on Laser Technology, Monterey, Calif., April, 1972, under the title "Optical Evaluation of CO_2 Laser Window Materials."

12. SPONSORING MILITARY ACTIVITY
Air Force Cambridge Research Laboratories (LQO)
L. G. Hanscom Field
Bedford, Massachusetts 01730

13. ABSTRACT

An overview of some of the theoretical and experimental aspects of the AFCRL optical evaluation program for high-power laser window materials is presented. A vector diffraction theory used to treat the thermal lensing problem is described. Absorption coefficient measurements on state-of-the-art window materials are presented, and problems encountered in optical evaluation by calorimetry are discussed. A new interferometric technique for measuring absorption coefficients of low optical loss materials is described.

DD FORM 1 NOV 65 1473

Unclassified
Security Classification

Unclassified

Security Classification

14. KEY WORDS	LINK A ROLE	LINK A WT	LINK B ROLE	LINK B WT	LINK C ROLE	LINK C WT
Laser window materials						
Infrared optics						
Diffraction optics						
Thermal lensing						
Interferometry						
Calorimetry						

Unclassified

Security Classification

AFCRL-72-0404
30 JUNE 1972
PHYSICAL SCIENCES RESEARCH PAPERS, NO. 500

SOLID STATE SCIENCES LABORATORY PROJECT 5621

AIR FORCE CAMBRIDGE RESEARCH LABORATORIES

L. G. HANSCOM FIELD, BEDFORD, MASSACHUSETTS

Some Aspects of Optical Evaluation of CO_2 Laser Window Materials at AFCRL

B. BENDOW
A. HORDVIK
H. LIPSON
L. SKOLNIK

Presented at the Fifth DoD Conference on Laser Technology, Monterey, California, April, 1972, under the title "Optical Evaluation of CO_2 Laser Window Materials."

Approved for public release; distribution unlimited.

AIR FORCE SYSTEMS COMMAND
United States Air Force

Abstract

An overview of some of the theoretical and experimental aspects of the AFCRL optical evaluation program for high-power laser window materials is presented. A vector diffraction theory used to treat the thermal lensing problem is described. Absorption coefficient measurements on state-of-the-art window materials are presented, and problems encountered in optical evaluation by calorimetry are discussed. A new interferometric technique for measuring absorption coefficients of low optical loss materials is described.

Contents

1. INTRODUCTION 1

2. THEORY OF THERMAL LENSING IN LASER WINDOW MATERIALS 2

3. EXPERIMENTAL 10

   3.1 Calorimetry 10

   3.2 Interferometry 18

4. SUMMARY 23

ACKNOWLEDGMENTS 25

REFERENCES 27

Illustrations

1. Coordinate System at Window and Near Observation Point P 3

2. Intensity vs Abstract Coordinates u and v, at Four Progressive Dimensionless Times C for a Material With $C_2\rho/C_1\rho = 0.1$, $C_1\theta/C_1\rho = 1.0$, and Amplitude $\propto e^{-6\rho^2}$ 5

3. Peak Intensity I_m, Average Intensity Within a Radius v = 12, I_{avg} and Beamwidth V_b, vs Dimensionless Time C, for Same Parameters as in Figure 2 6

4. On-axis Intensity Distribution at Ten Progressive Times, for KCl and CdTe 7

Preceding page blank

Illustrations

5. Maximum Intensity vs Time for CdTe, KCl, NaCl, KI and NaCl-KI Composite, for Parameters Indicated 7

6. Typical Thermal Rise and Decay Curve 11

7. Thermal Rise and Decay Curves for Harshaw KCl Crystal 13

8. Thermal Rise and Decay Curves for $KCl_{0.32}Br_{0.68}$ Crystals 14

9. Absorption Coefficient Variations in Polished and Cleaved KCl Crystals 15

10. Absorption Coefficient Variation With Position in CdTe Crystal 16

11. Twyman-Green Interferometer Used for Measuring Absorption Coefficients of Low-Loss Materials 19

12. Fringe Count vs Temperature Rise Calibration Curve for a KBr Window Obtained on the Apparatus of Figure 11 19

13. Time Dependence of Twyman-Green Interference Patterns of a KBr Window With 900 W/cm^2 Incident CO_2 Radiation 22

Tables

1. Material Parameters at 10.6 μm 9

2. Optical Performance of Laser Window Materials at 10.6 μm (P_o = 500 W/cm^2, L_o = 2 cm) 10

3. Absorption Coefficients of State-of-the-Art Materials 17

Some Aspects of the Optical Evaluation of CO_2 Laser Window Materials at AFCRL

1. INTRODUCTION

The evaluation of far infrared transmitting materials for use as high power CO_2 laser windows has received considerable attention in recent years (Sahagian and Pitha, 1971a). In particular, recent progress in the development and exploitation of high-power output laser systems has disclosed serious material limitations which can lead to optical failure of the window prior to the onset of observable physical damage. Optical performance of the window may be degraded by absorption processes, scattering mechanisms or thermal distortion effects which cause the window to act as an aberrating lens. It is these "thermal lensing" phenomena which may place a fundamental limitation on the use of high-power laser systems.

AFCRL is presently involved in the growth, and physical and optical characterization of new materials for infrared laser windows. This paper provides an overview of some of the theoretical and experimental aspects of the optical evaluation program for laser window materials. A vector diffraction theory of aberration which supplies the detailed three-dimensional laser beam intensity distribution in all space and for all times is used to treat the thermal lensing problem. Calorimetric measurements of absorption coefficients for window materials grown at AFCRL and other facilities are presented, and the influence of sample homogeneity

(Received for publication 29 June 1972)

on calorimetric data is demonstrated. Finally, a new interferometric technique for measuring low absorption coefficients is described and the application of interferometry to window device evaluation is discussed.

2. THEORY OF THERMAL LENSING IN LASER WINDOW MATERIALS

The absorption of energy from a non-uniform laser beam incident on a sample leads to the imposition of a non-uniform temperature distribution in the sample (Sparks, 1971; and Jasperse and Gianino, 1972). Due to the dependence of the refractive index on temperature, the effective optical path length in the sample becomes a function of position, and the sample acts as an aberrating lens. In addition, the faces of the sample bulge, further contributing to the lensing effect. Finally, induced stresses lead to position dependent changes in the refractive index. These various effects cause distortion and defocussing of laser beams traversing solid samples, conventionally referred to as "thermal lensing".

Due to stress-induced effects present in many potential window materials, it is necessary to adapt vector (Jackson, 1962), rather than scalar wave theory to describe lensing. One may show (Bendow et al, 1971-72) that the vector Kirchhoff approximation leads to the following expression for the field $\vec{U}$ beyond a thin circular sample:

$$U = U_1\hat{\epsilon}_1 + U_2\hat{\epsilon}_2 ,$$

$$U_1(u,v) = 2\pi\int_0^1 d\rho\rho E_1(\rho)[J_0(\rho v)\exp(ik\Phi_\rho) - J_1(\rho v)(\exp(ik\Phi_\rho)-\exp(ik\Phi_\theta))/\rho v] \times \exp\left(-\frac{iu\rho^2}{2}\right),$$

$$U_2(u,v) = 2\pi\int_0^1 d\rho\rho E_2(\rho)[J_0(\rho v)\exp(ik\Phi_\theta) + J_1(\rho v)(\exp(ik\Phi_\rho)-\exp(ik\Phi_\theta))/\rho v] \times \exp\left(-\frac{iu\rho^2}{2}\right),$$

where Φ_ρ and Φ_θ are the aberration functions (Born and Wolf, 1964) characterizing ρ and θ polarized radiation, $E_1\hat{\epsilon}_1 + E_2\hat{\epsilon}_2$ is the incident field on the sample, and the E_i's have been taken to be functions of radial position alone. The coordinates (u, v) are defined by

$$u \equiv ka^2(x_0^{-1} - x^{-1}),$$

$$v \equiv ka\rho' x^{-1} ,$$

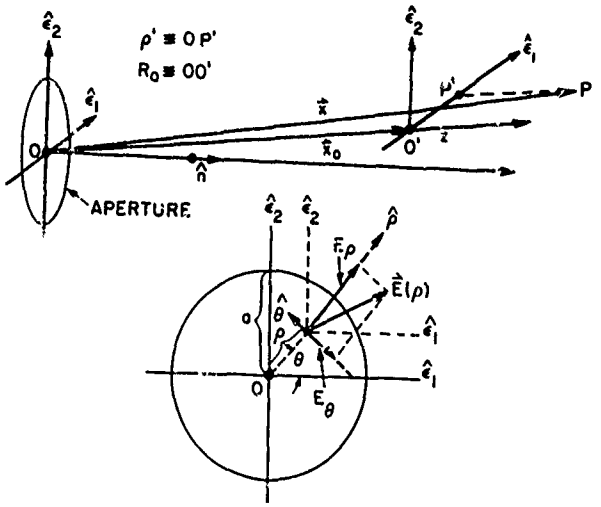

Figure 1. Coordinate System at Window and Near Observation Point P. O' is the Gaussian prefocus

with k the wave vector and a the window radius. The coordinate system employed is depicted in Figure 1. We note that the form given is appropriate in the small angle approximation.

Following Sparks (1971) and Jasperse and Gianino (1972), for example, one may derive the functions Φ_ρ and Φ_θ, which take the following form in terms of the thermal distribution $\Delta T(\rho, t)$, with t the time:

$$\Phi_{\rho,\theta}(\rho, t) = aS_2^{\rho,\theta} \langle \Delta T \rangle_z + 4aS_2^{\rho,\theta} \int_0^\rho x \langle \Delta T \rangle_z dx/\rho^2 ,$$

where we have omitted a constant term which does not effect the value of the intensity. $\langle \ \rangle_z$ indicates an average with respect to the z direction (across the thickness). One finds

$$S_1^\rho = \frac{\partial n}{\partial T} + \bar{\alpha}\frac{n^3}{2}[(1-\nu)p_{12} - \nu p_{11}] + \bar{\alpha}(1+\nu)(n-1) ,$$

$$S_2^\rho = \bar{\alpha}\frac{n^3}{8}(1-\nu)(p_{11} - p_{12}) ,$$

$$S_1^\theta = S_1^\rho \{[(1-\nu)p_{12} - \nu p_{11}] - [p_{11} - 2\nu p_{12}]\} ,$$

$$S_2^\theta = -S_2^\rho .$$

Here n is the refractive index, $\partial n/\partial T$ is taken at zero-stress, $\bar{\alpha}$ is the thermal expression coefficient, ν is Poisson's ratio, and the p_{ij}'s are stress-optic coefficients. It may be shown that for isolated (uncooled) windows, the linear time approximation to ΔT applies in the time regime of interest. Neglecting variations along the window thickness, in this regime one obtains for a Gaussian beam:

$$\Phi_{\rho,\theta} = C_1^{\rho,\theta} e^{-2\alpha^2\rho^2} + C_2^{\rho,\theta}(1-e^{-2\alpha^2\rho^2})/\alpha^2\rho^2 ,$$

where the incident amplitude

$$\propto e^{-a^2\rho^2} ,$$

and

$$C_i^{\rho,\theta} = L_o P_o \beta t S_i^{\rho,\theta}/C' ,$$

with L_o the window thickness, β the bulk absorption coefficient, P_o the incident peak power, and C' the specific heat times the density. Analogous results for Φ may be derived for other beam geometries as well.

A convenient quantity to investigate is the power per unit solid angle at the observation point relative to its initial value at the Gaussian prefocus. We refer to this quantity as the "intensity" and it is given by

$$I(u,v,t) = \frac{|U_1|^2 + |U_2|^2}{|2\pi\int_0^1 d\rho\rho E_1(\rho)|^2 + |2\pi\int_0^1 d\rho\rho E_2(\rho)|^2} .$$

For a linearly polarized Gaussian beam, one obtains

$$I = \frac{\alpha^4}{\pi^2} \frac{|U_1|^2\cos^2\psi + |U_2|^2\sin^2\psi}{\left(1 - e^{-\alpha^2}\right)^2} ,$$

where ψ is the angle between $\hat{e}_1$ and the incident field. For an unpolarized beam, one replaces $\sin^2\psi$ and $\cos^2\psi$ by 1/2.

A pictorial representation of lensing may be obtained by displaying the full intensity distribution I(u, v) at consecutive values of the abstract time $C \equiv C_1^{\rho}$. This is illustrated in Figure 2. One notes that as time increases, the maximum intensity degrades, the beam spreads and diffuses over a larger region of space,

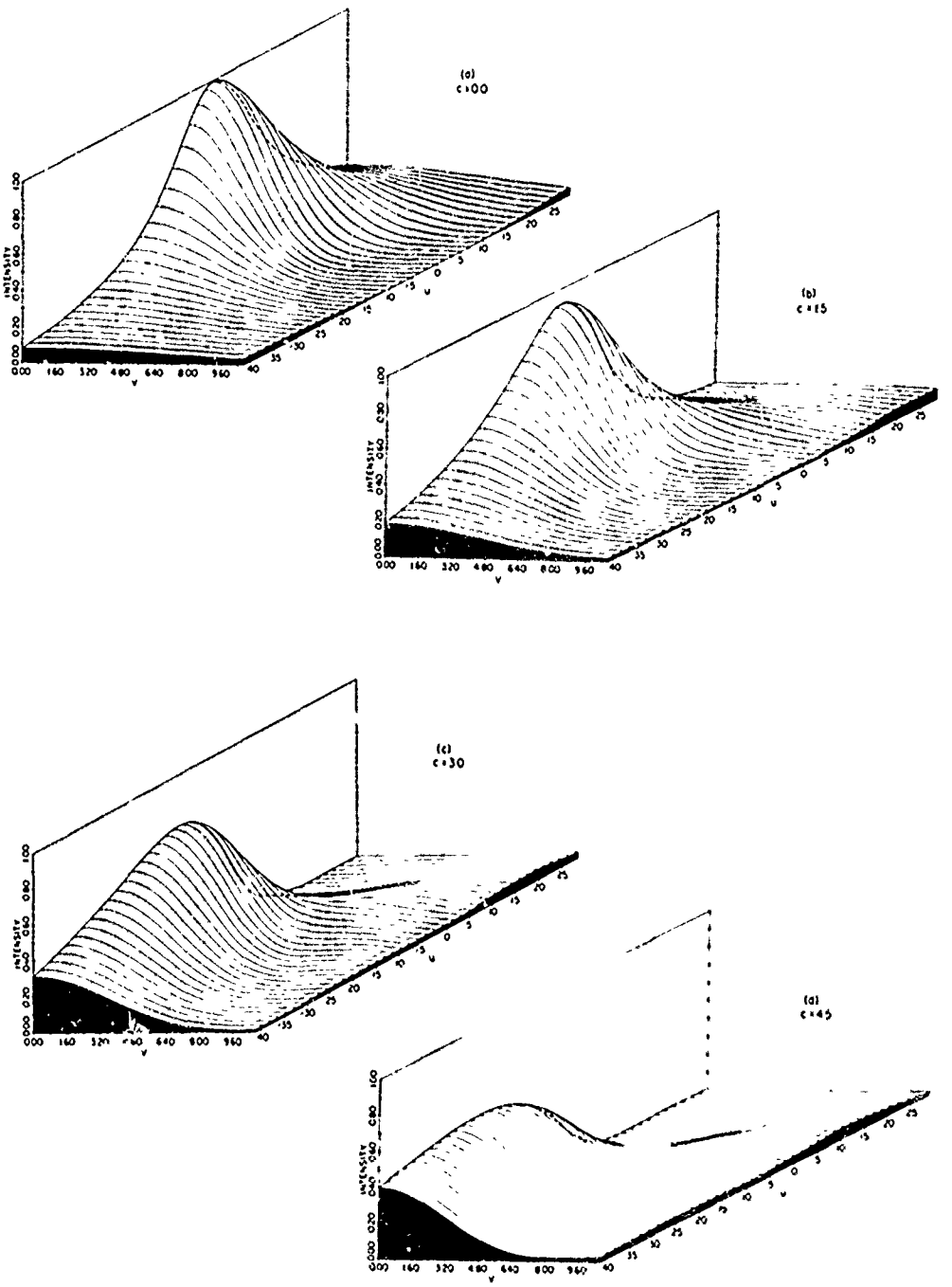

Figure 2. Intensity vs Abstract Coordinates u and v, at Four Progressive Dimensionless Times C for a Material With $C_2^{\rho}/C_1^{\rho}=0.1, C_1^{\theta}/C_1^{\rho}=1.0$, and Amplitude $\propto e^{-6\rho^2}$

and the diffraction focal point shifts away from the initial Gaussian prefocus. There are a variety of ways of expressing the beam degradation. In Figure 3, for example, the maximum intensity, the average intensity within a fixed radius, and the effective beamwidth are plotted versus abstract time. The decrease in intensities with time and the increase of the beamwidth provide complementary descriptions of the beam degradation.

For simplicity, it is often useful to consider just the evolution of the on-axis intensity distribution [Bendow and Gianino (1972)] as a function of time. In Figure 4 we display the on-axis distribution at ten successive times for KCl and CdTe. Note that KCl is a "diverging" material, while CdTe is "converging". The on-axis distribution is especially useful for extracting the maximum intensity as a function of time for various materials. In Figure 5 we display the intensity degradation for four materials. In addition, the behavior of a composite lens of compensating layers of NaCl and KI, one which is converging and the other diverging, is illustrated. From the figure it is evident that the three alkali-halides are substantially superior optically to CdTe. In addition, the composite window yields an optical performance nearly an order of magnitude better than that of the individual constituents.

It can be shown that the defocussing effect may be compensated for by an appropriate time-dependent refocussing (Bendow and Gianino, 1972). On the other hand, the intensity degradation cannot be averted and thus becomes the dominant failure mode in the optical performance. The classical "aberration criterion" for the performance of a lens is the maintenance of the maximum intensity to a specified fraction of the initial intensity. For example, Marechal's criterion

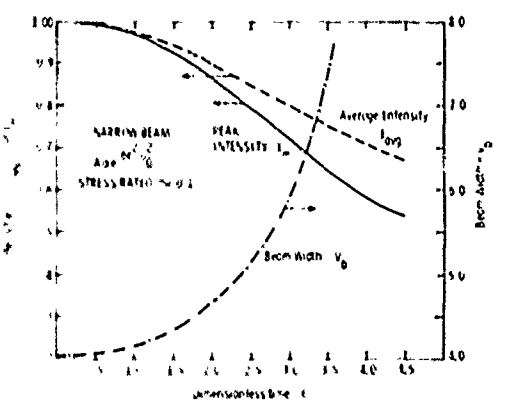

Figure 3. Peak Intensity Im, Average Intensity Within a Radius v = 12, I_{avg}, and Beamwidth Vb, vs Dimensionless Time C, for Same Parameters as in Figure 2

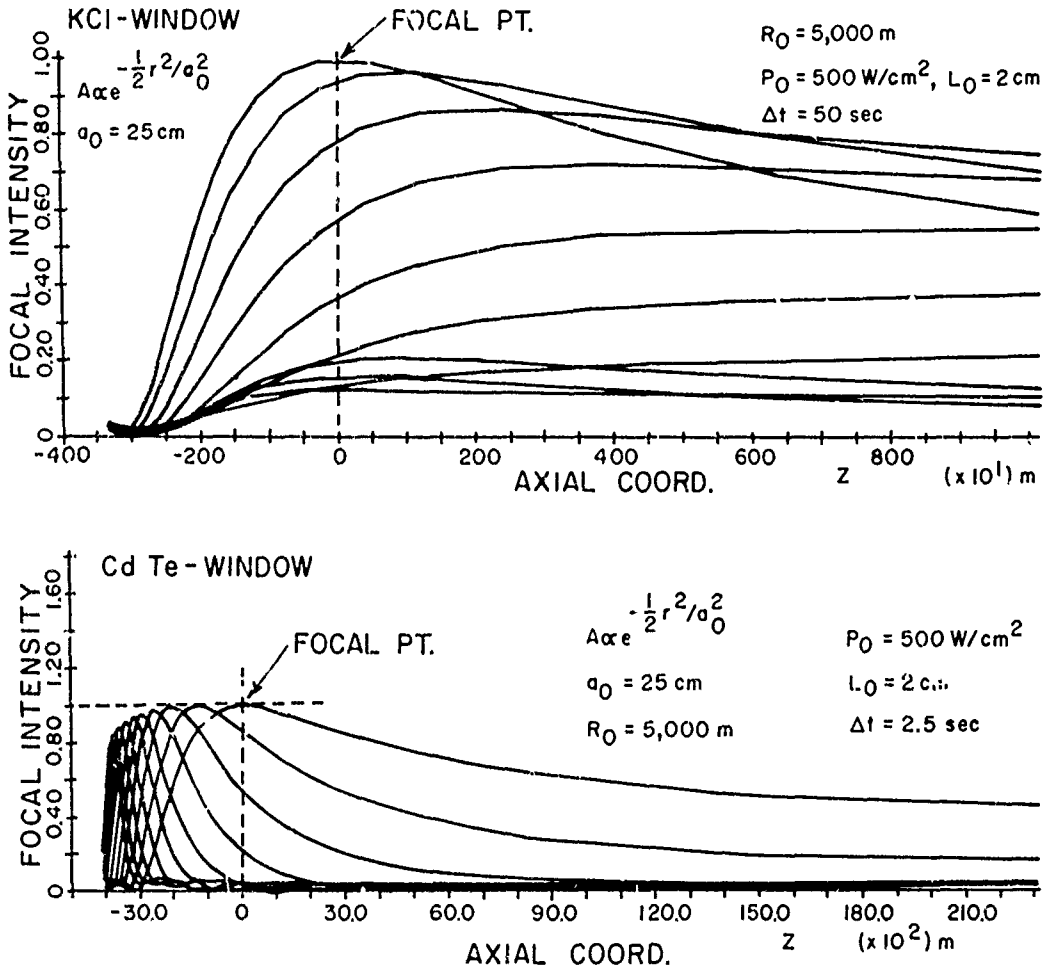

Figure 4. On-axis Intensity Distribution at Ten Progressive Times, for KCl and CdTe. Parameters employed are indicated in the figure

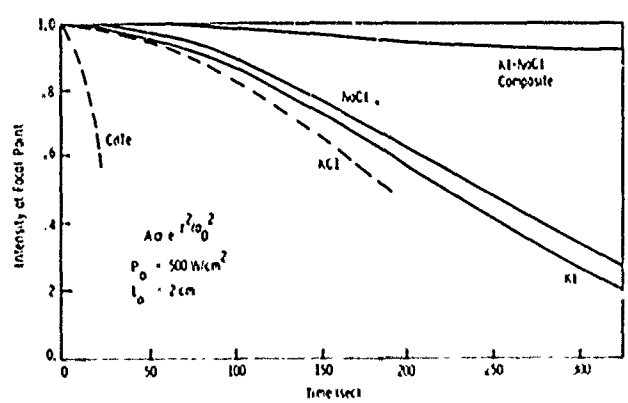

Figure 5. Maximum Intensity vs Time for CdTe, KCl, NaCl, KI and NaCl-KI Composite, for Parameters Indicated

(Born and Wolf, 1964) considers a system "aberrated" when $I \rightarrow 0.8\ I_o$. In this spirit, we define the degradation time t_f in which the maximum intensity degrades to f times its initial value; the larger t_f, the better the optical performance. As the quantity f is arbitrary and varies with the application, we will choose as an example the 90 percent degradation time $t_{0.9}$. (The relative performance of the various materials will not vary very much with f, although of course the absolute magnitude of t_f will.) By employing values for the material parameters displayed in Table 1, one is able to compute a table of values of $t_{0.9}$ for different materials, and for different beamshapes α. In Table 2 we present values for $t_{0.9}$ at 10.6 μm for a variety of materials, and two beams, one wider and one narrower with respect to the window. It may be concluded that as a class, alkali-halides are substantially superior in optical performance to semiconductors and glasses. From among the alkali-halides, KBr appears to be markedly superior. It must be noted, however, that the predicted values depend critically on a variety of material parameters, some of which are not accurately known. Thus some adjustments in relative ratings are certainly possible when better values for these parameters become available. We also note the dependence of relative ratings on beamwidth, due to diffraction effects. For the values of P_o and L_o indicated, characteristic degradation times are in the hundreds of seconds for alkali-halides, and in the tens for semiconductors. These values scale inversely with P_o and L_o; as one goes to a higher power P'_o and larger thickness L'_o, $t_f \rightarrow (P_o/P'_o)(L_o/L'_o)t_f$. This inverse scaling illustrates the difficulty of maintaining required intensities at the target at higher powers, and under conditions where mechanical constraints require greater window thicknesses.

As data becomes available* on new materials and as better values are obtained for existing materials, it is believed that the present analysis can be usefully applied to predict just which materials perform best optically. Thus, when combined with appropriate experimental verification, this approach can provide a comprehensive and rigorous basis for the selection of laser window materials.

---

* For a collection of current values, see "Compendium on High Power IR Laser Materials", C. Sahagian and C. Pitha, Eds., AFCRL-72-0170 (1972).

Table 1. Material Parameters at 10.6 μm

Material		$C'\left(\frac{J}{cm^3 {}^oK}\right)$	$\bar{\alpha}({}^oK)^{-1} \times 10^5$	$K\left(\frac{W}{cm\,{}^oK}\right) \times 10^2$	n	$\beta(cm^{-1}) \times 10^3$	$P_{11} \times 10$	$P_{12} \times 10$
I-VI	KBr	1.20	4.30	4.80	1.53	0.05	2.15	1.68
	KCl	1.35	3.60	6.53	1.46	2.7	2.09	1.56
	NaCl	1.85	4.40	6.49	1.49	1.34	1.26	1.68
	KI	0.983	4.26	2.50	1.62	*1.0	2.13	1.72
	CsI	0.906	5.00	1.13	1.74	1.3	-	-
	CsBr	1.17	4.79	0.96	1.66	4.4	-	-
	KRS-5	*1.45	5.80	0.54	2.37	5.0	*2.0	*2.0
II-VI	CdTe	1.37	0.45	4.10	2.60	1.6	*1.5	*0.0
	ZnSe	0.379	0.70	12.14	2.40	*6.0	*1.5	*0.0
III-V	GaAs	1.55	0.60	46.00	3.30	12.0	-1.65	-1.40
	InSb	1.20	0.49	20.00	3.95	8.6	*2.0	*2.0
IV	Ge	1.65	0.60	60.00	4.00	19.0	2.7	2.35
Glasses								
TI Glass 1173		1.29	1.50	0.30	2.60	20.0	*2.0	*2.0
TI Glass 20		1.33	1.33	0.26	2.49	*30.0	2.1	2.1
Polycrystals								
IRTRAN-4		2.65	0.80	12.98	2.41	122	*1.5	*0.0
IRTRAN-6		1.22	0.57	4.10	2.67	120	*1.5	*0.0

Note: * Estimated

Table 2. Optical Performance of Laser Window Materials at 10.6 μm (P_o = 500 W/cm^2, L_o = 2 cm)

Material	$t_{90\%}$ (sec): Time in which maximum intensity degrades to 90% initial value	
	Wider Beam $A \propto e^{-1/2}\rho^2$	Narrower Beam $A \propto e^{-3}\rho^2$
KBr	3220	1670
KCl	75	60
NaCl	190	47
KI	125	38
CsI	36	5.5
CsBr	27	4.2
CdTe	16	2.4
ZnSe	2.5	0.4
Ge	0.6	0.1
IRTRAN-4	0.6	0.1
IRTRAN-6	0.1	0.02

3. EXPERIMENTAL

3.1 Calorimetry

In this section we describe aspects of the experimental optical evaluation program at AFCRL. These have currently centered principally about calorimetric measurements of absorption coefficients, and application of interferometric techniques for studying absorption and for device evaluation. We discuss these programs and certain of the results below.

3.1.1 CALORIMETRIC EQUIPMENT AND TECHNIQUES

Calorimetry equipment is in operation at AFCRL for routine measurements of small absorption coefficients at 10.6 μm. The calorimeter consists of a large aluminum cylinder with feedthroughs for thermocouples, evacuation ports, and mounts for windows. A special feature is a bellows sample mount which allows accurate positioning of different regions of samples in the beam for scanning purposes. A 5-watt stable CO_2 laser is directed either through apertures to

limit the beam or through a Ge focussing lens. Both the initial laser power and that transmitted through the sample is measured with a disc-type calorimetric power meter. Thermocouple voltages are measured during the thermal rise and decay periods, amplified by a dc nanovoltmeter, and recorded.

Although the equipment was designed for evacuated adiabatic calorimetry, most measurements are made in air without windows. Comparative measurements have shown that when both rise and decay rates are properly considered, identical results for absorption coefficients are obtained in vacuum and in air. Also, elimination of windows removes the possibility of scattering of laser radiation from window surfaces and allows a more sensitive determination of bulk or surface scattering occurring within the crystal.

Sample surfaces are prepared either by polishing or cleaving. The most reproducible results are obtained when thermocouples are attached either to optically polished or as-grown surfaces. Thermocouples are usually placed on opposite sides of the sample equidistant from the laser beam. The presence of scattered laser radiation which produces direct heating of the thermocouples is evidenced by a steep slope in the thermal rise curve just after laser turn-on, and a corresponding slope in the decay curve after turn-off. Good agreement of thermal rise and decay rates for thermocouples placed on opposite sides of the sample is also an indication that directional scattering is not present.

3.1.2 ANALYSIS OF THERMAL RISE AND DECAY CURVES

A typical thermal rise and decay curve obtained when the laser heats the sample for a given period of time and is then turned off is shown in Figure 6.

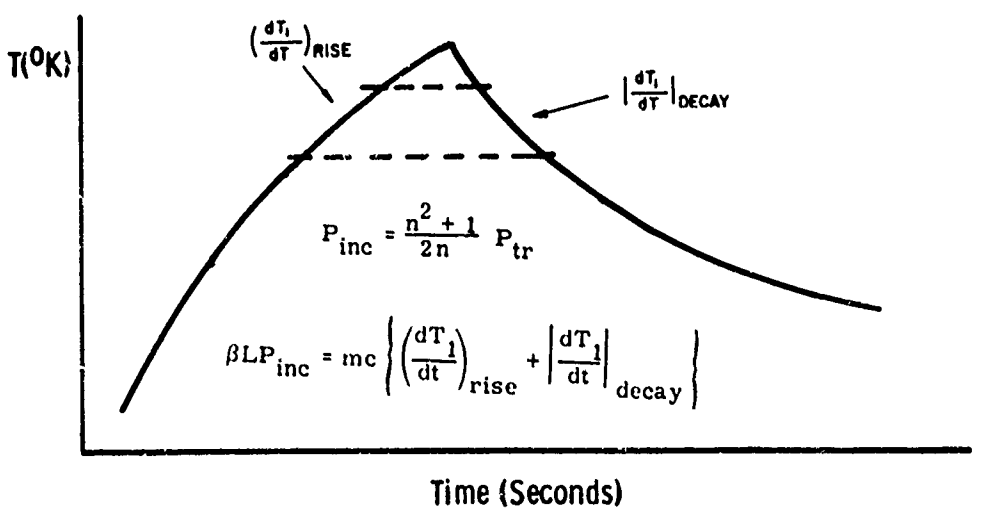

Figure 6. Typical Thermal Rise and Decay Curve

The heat absorbed in the sample is determined from the sum of the (dT_1/dt) rise and $|dT_1/dt|$ decay slopes measured over the same temperature interval as indicated by the dashed lines. For most samples the sum of the rise and decay slopes are nearly constant over the temperature range of measurement unless some other mechanism such as scattering is operative.

The absorption coefficient designated as β (or β_A) is determined from the expression

$$\beta L P_{inc} = mc\left[\left(\frac{dT_1}{dt}\right)_{rise} + \left|\frac{dT_1}{dt}\right|_{decay}\right],$$

where

T_1 = temperature above ambient,

L = sample length,

P_{inc} = incident power,

m = sample mass,

c = specific heat.

The power incident on the sample is either measured without the sample in place or determined from the transmitted power by the relation

$$\frac{P_{tr}}{P_{inc}} = \frac{(1-R)^2 e^{-\beta d}}{1-R^2 e^{-2\beta d}},$$

where R = bulk reflectivity, and d = sample thickness. For small absorption coefficients $e^{-\beta d} \approx 1 - \beta d$ and

$$\frac{P_{tr}}{P_{inc}} = \frac{(1-R)^2(1-\beta d)}{1-R^2(1-2\beta d)}.$$

With absorption coefficients small enough for $1-\beta d \approx 1$, the expression reduces to that shown in Figure 6

$$\frac{P_{tr}}{P_{inc}} = \frac{(1-R)^2}{1-R^2} = \frac{2n}{n^2+1}$$

where n = index of refraction, since for the above approximations $R = \frac{(n-1)^2}{(n+1)^2}$.

3.1.3 ABSORPTION OF SINGLE CRYSTAL KCl AND POLYTRAN KCl

Thermal rise and decay curves are shown in Figure 7 for a polished sample of Harshaw KCl. The difference in absorption coefficients, measured for thermocouples placed at the positions shown on the top polished surface of the crystal, is attributed to a small amount of direct radiation (in this case reflected from the calorimeter windows) reaching the front and rear thermocouples. The thermal rise and decay curves of these thermocouples show the steep slope regions characteristic of direct heating. These additional slopes are not present in the curves of the center thermocouple for which the lowest rise and decay rate of $0.037^{\circ}K/W$ min and absorption coefficient $\beta_A = 0.0053\ cm^{-1}$ is measured.

From similar measurements on Harshaw Polytran KCl, we have determined that material grown by this process with its greater strength capability has absorption equivalent to single crystal KCl. Absorption coefficient values of $0.0040 \pm 0.0010\ cm^{-1}$ were determined for a sample with polished faces normal to the laser beam and rough ground faces for attachment of thermocouples. The absorption coefficient variation was between thermocouples placed on different

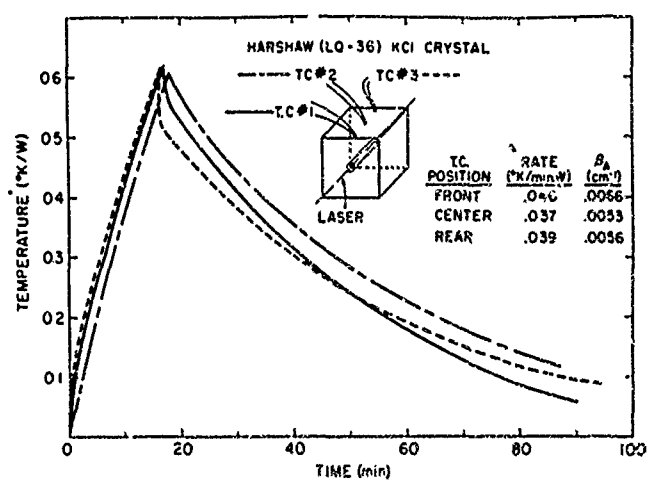

Figure 7. Thermal Rise and Decay Curves for Harshaw KCl Crystal

faces equidistant from the laser beam and may have resulted from thermocouple-surface contact or possibly some internal inhomogeneity. With better surfaces and improved material, even lower absorption coefficients may be found.

3.1.4 EFFECT OF IMPERFECTIONS ON CALORIMETRIC MEASUREMENTS OF ABSORPTION COEFFICIENT

With the emphasis of the AFCRL program on the development of new CO_2 laser window materials, an important aspect of characterization is measurement of small samples and small regions of larger samples to determine homogeneity. Our calorimetric measurement equipment has been developed along these lines and our measurements demonstrate that imperfections can produce scattering of the laser radiation and regions of higher absorption in a crystal.

Figure 8 shows the thermal rise and decay curves for a crystal of $KCl_{0.32}Br_{0.68}$ (LQ-97)* grown at AFCRL. This material has a hardness close to three times that of either KCl or KBr, but still has a relatively low absorption coefficient. The sample surfaces normal to the laser beam were cleaved while those to which thermocouples were attached were in the as-grown condition. Measurements with different size beams demonstrate the effect of a small imperfection visible within the crystal lying close to the front surface. With no windows

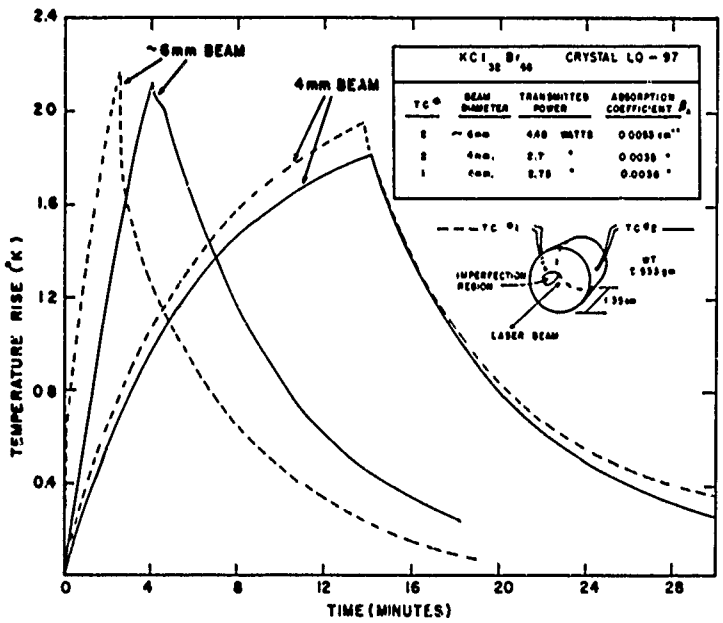

Figure 8. Thermal Rise and Decay Curves for $KCl_{0.32}Br_{0.68}$ Crystals

* ALQLOY (patent applied for)

and a 4-mm aperture limiting the laser beam to a region which covered very little of the imperfection, very similar rise and decay curves are seen for both thermocouples. With the beam widened to ~6 mm and intercepting the imperfection, steeper rise and decay slopes, after normalization to $^{o}K/W$, are observed and a correspondingly larger absorption coefficient is measured. A value of 0.0053 cm^{-1} is found as compared to 0.0036 cm^{-1} when the imperfection region is avoided. A pronounced steep slope region, probably due to direct heating through scattered radiation, is seen in the rise and decay curves of the thermocouple closest to the imperfection.

The data of Figure 9 demonstrates the effect of a planar imperfection on calorimetry results. A rectangular sample 1.27 × 1.27 × 2.54 cm polished on all sides was prepared from a crystal of AFCRL grown KCl (LQ-50). Absorption measurements made with a focussed beam of 1-mm diameter through the center of the long dimension gave a value of 0.0038 cm^{-1} with excellent agreement for thermocouples placed on different sides of the sample. A much larger absorption coefficient, 0.0077 cm^{-1}, was measured with the beam directed through the center of the shorter dimension.

When examined interferometrically with a helium-neon laser, a scattering surface extending through the long dimension of the crystal and slightly displaced from the center was observed. The increase in absorption with the laser directed through the shorter dimension is attributed to the beam passing through this imperfection region.

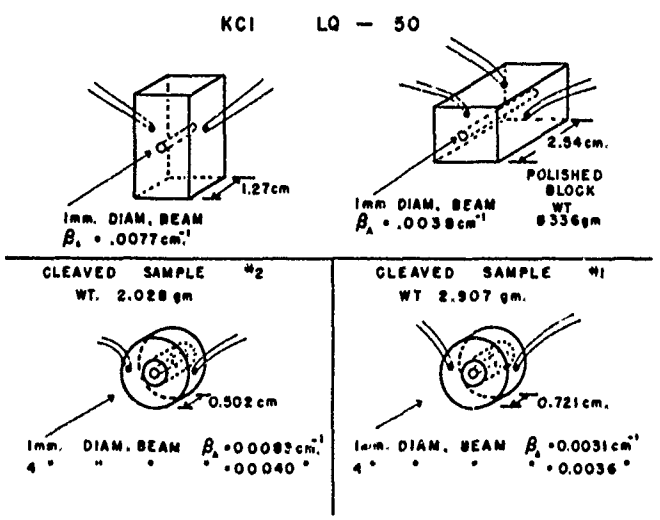

Figure 9. Absorption Coefficient Variations in Polished and Cleaved KCl Crystals

Absorption coefficient measurements on cleaved sections taken from the same crystal indicate that this imperfection did not extend throughout the boule. Measurements were made with a 1-mm focussed beam and a wider 4-mm beam directed normal to the cleaved surface. Little difference was observed between absorption coefficients determined when the beam covered different areas near the center of sample #1. The absorption coefficient values ranging from 0.0031 to 0.0036 cm^{-1} were also in good agreement with that measured for the long dimension of the polished sample.

A different result was obtained with different size beams for sample #2 which must have contained an imperfection within the region of measurement. An absorption coefficient of 0.0040 cm^{-1} was obtained with the 4-mm beam size. When the beam was focussed to 1 mm, however, a value of 0.0083 cm^{-1}, comparable to that measured for the short dimension of the polished sample, was found. The higher absorption coefficient probably arises from concentration of the most intense part of the beam into the imperfection region.

The problem of inhomogeneity in absorption at 10.6 μm is also found for other potential window materials. A large sample of CdTe was sent to a number of laboratories engaged in calorimetric measurements as part of a "round robin"

CdTe #1

T C #	BEAM POSITION	AVERAGE TRANSMITTED POWER	ABSORPTION COEFFICENT β_A
1	CENTER	3.075 WATTS	0.0975 cm^{-1}
2	" "	3.250 "	0.1118
1	5MM.BELOW CENTER	3.350 "	0.0306
2	" "	3.350 "	0.0238

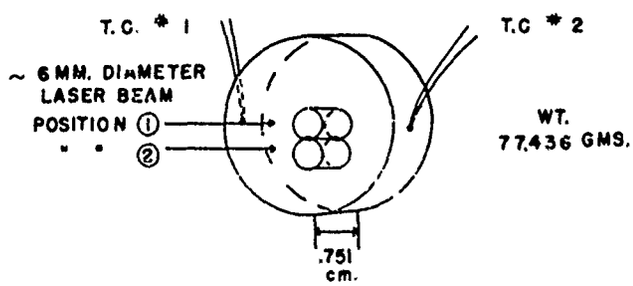

Figure 10. Absorption Coefficient Variation With Position in CdTe Crystal

sponsored by AFML. A wide variation of absorption coefficient values ranging from 0.024 to 0.414 cm^{-1} were obtained for this sample by the different laboratories. Our measurements with a 6-mm diameter beam positioned at the center gave the values shown in Figure 10, or an average value of 0.105 ± 0.007 cm^{-1}. With the beam positioned 5 mm below the center of the sample, a much lower absorption coefficient is found with an average value of 0.027 ± 0.0035 cm^{-1}. The absorption coefficient of this sample at 10.6 μm is seen to be very non-uniform, varying by nearly a factor of four over a relatively small region close to the center.

3.1.5 ABSORPTION COEFFICIENTS OF STATE-OF-THE-ART MATERIALS

Calorimetric measurements of absorbed power thus provide a sensitive determination of absorption coefficient at 10.6 μm. These techniques can also be extended to study homogeneity in crystals and other materials useful for CO_2 laser windows. The materials investigated to date at AFCRL and absorption coefficients found from our measurements are listed in Table 3. These values have been determined from an average of results where good agreement has been obtained between two or more thermocouples. The absorption coefficients listed are for sections of samples which do not contain flaws or other localized regions of strong absorption or scattering. Also listed in Table 3 is the condition of surfaces normal to the laser beam. Absorption coefficients of Table 3 are for samples measured at AFCRL and may not agree with literature values of Table 1.

Table 3. Absorption Coefficients of State-of-the-Art Materials

Sample	Surface Condition	Absorption Coefficient β_A (cm^{-1})
KCl (Harshaw)	Polished	0.0059
KCl (Harshaw Polytran)	Polished	0.0040
KCl (AFCRL)	Polished	0.0040
KCl (AFCRL)	Cleaved	0.0030
$KCl_{0.32}Br_{0.68}$ (AFCRL)*	Cleaved	0.0035
KBr (Commercial Window)	Polished	0.0030
KBr (AFCRL)	Polished	0.0040
ZnSe #4 (Round Robin)	Polished	0.058
ZnSe (IRTRAN-4)	Polished	0.048
CdTe #6 (Round Robin)	Polished	0.0045
CdSe (ARL)	Polished	0.016
GaAs (Monsanto)	Polished	0.015

Note: * ALQLOY (patent applied for)

3.2 Interferometry

3.2.1 ABSORPTION COEFFICIENT MEASUREMENTS

Although calorimetry is a sensitive method for the determination of small absorption coefficients, the results of the previous section indicate some of the problems that arise with these measurements. Difficulties encountered in thermocouple placement and attachment, surface and bulk absorption, and internal and surface scattering complicate the interpretation of calorimetric data. In this section, we discuss a new technique for measuring absorption coefficients of low-loss materials which can minimize some of the problems encountered in conventional calorimetry. This technique, shown in Figure 11, utilizes an interferometer such as the Twyman-Green or Mach-Zender type. The method employs a frequency stabilized He-Ne probe beam, but other lasers may be used as long as the sample is transparent to the probe beam radiation. The technique, based on the number of interference fringes counted, can be made more sensitive by using shorter wavelength probe beams. The method consists of inserting the window sample in a furnace into one leg of the interferometer and observing the fringe shift as a function of sample temperature. Subsequently, when the sample is heated by absorbing CO_2 laser radiation, the fringe shift versus temperature calibration serves as a remote "thermocouple" to sense window temperature rise.

If a sample of uniform thickness and refractive index is inserted into one leg of the interferometer, then constructive interference occurs whenever the optical path difference is an integral number of wavelengths, or

$$2Ln = K\lambda \,, \tag{1}$$

where

L is the window thickness,
n is the refractive index,
K is an integer,
λ is the probe radiation wavelength.

(The factor of 2 arises because the Twyman-Green interferometer is of the double pass type.) If the sample is uniformly heated, the fringe pattern will traverse the center of the field because of changes in refractive index and thickness. The fringe shift observed per degree temperature change is found from Eq. (1) to be:

$$\frac{\Delta k}{\Delta T} = \frac{2Ln}{\lambda}\left(\frac{1}{n}\frac{dn}{dT} + \frac{1}{L}\frac{dL}{dT}\right). \tag{2}$$

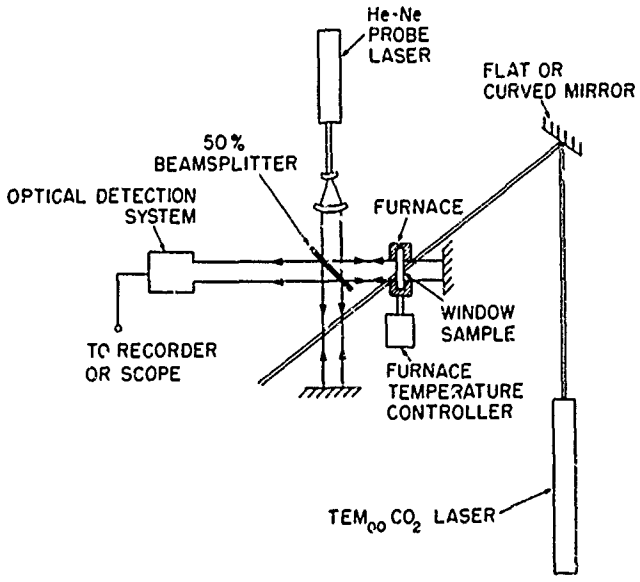

Figure 11. Twyman-Green Interferometer Used for Measuring Absorption Coefficients of Low-loss Materials. The apparatus is shown with a He-Ne probe laser and CO_2 heating laser

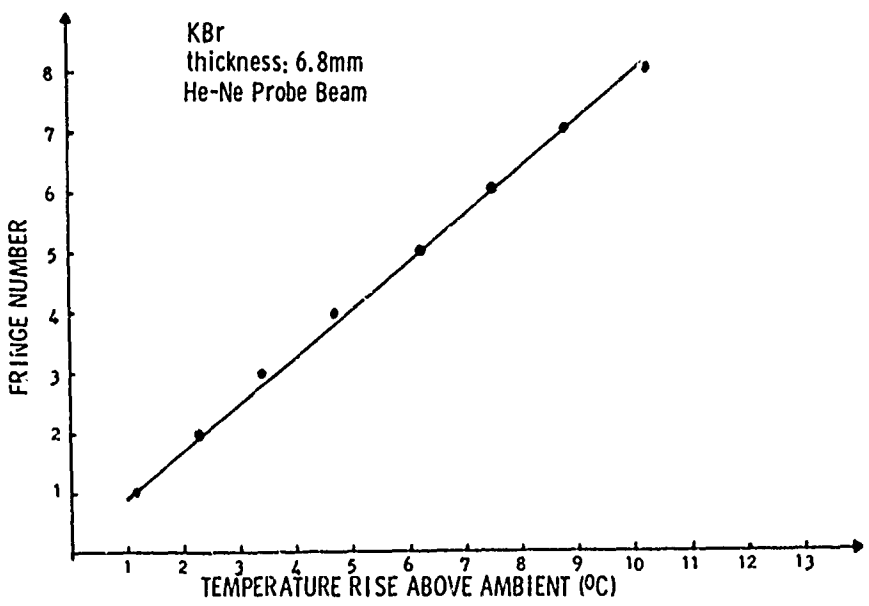

Figure 12. Fringe Count vs Temperature Rise Calibration Curve for a KBr Window Obtained on the Apparatus of Figure 1

If the sum of the temperature coefficient of refractive index $\left(\frac{1}{n}\frac{dn}{dT}\right)$ and the expansion coefficient $\left(\frac{1}{L}\frac{dL}{dT}\right)$ is constant over some small temperature range, then the fringe shift varies linearly with temperature. The slope of the fringe number versus temperature curve is given by Eq. (2). A representative calibration curve obtained with a 6328 Å probe beam is shown for a KBr sample in Figure 12. The data were generated by uniformly heating the sample with a resistance furnace and monitoring the temperature rise at the point where the He-Ne probe beam passes through the window. After this calibration curve is obtained, the CO_2 laser is aligned so that its beam path is nearly collinear with that of the probe beam. The sample is then heated with the CO_2 laser beam and the fringe pattern movement is monitored as a function of time. From the previous calibration curve, the corresponding temperature versus time curve is derived, and the absorption coefficient at 10.6 μm is calculated.

We mention here several advantages of this interferometric technique over conventional calorimetry:

(1) The need for temperature sensors attached to the sample is eliminated. Absorption coefficients are determined for the actual area through which the CO_2 laser passes.

(2) Measurements can be performed in the small time region (less than a characteristic thermal diffusion time) before edge heat losses and other non-symmetry effects become important. Therefore, thermal decay need not be a consideration (see paragraph 3.1).

(3) Calculations of the three-dimensional heat flow equation reduce to the $r = 0$ case and become independent of sample geometry.

(4) If the expansion coefficient is known, the same general apparatus can be used to determine the temperature dependence of the refractive index [see Eq. (2)]. Also, a separate interferometric technique can be used to evaluate the expansion coefficient (Foster and Osterink, 1968).

(5) Absorption variations due either to local compositional or refractive index inhomogeneities can be evaluated by scanning the probe and/or heating beams across the window. Similarly, various regions can be investigated for non-uniform heating effects.

(6) Measurement sensitivities can be increased by increasing sample length and by decreasing probe beam wavelength. (Focussing the CO_2 beam is limited, however, by thermal induced stress-optic effects as described below.)

(7) It may become possible to separate bulk and surface absorption by passing the CO_2 lasing beam perpendicular to the probe beam.

Thus far, interferometric measurements have yielded absorption coefficients consistently smaller than those found by standard calorimetry. For example, the

absorption coefficient for the KBr sample whose calibration data is shown in Figure 12 was found to be $\sim 1\times10^{-3}$ cm^{-1} interferometrically, while calorimetry gave a value of $\sim 3\times10^{-3}$ cm^{-1}. This discrepancy may be partially a result of the failure of the calibration technique to consider stress-optic effects thermally induced by the Gaussian CO_2 laser beam. For alkali-halides these stress-induced effects may be on the same order as the temperature variational effects, especially if a sharply focussed CO_2 heating beam is used (Horrigan and Deutsch, 1971). If one or more of the stress-optic coefficients are reversed in sign to that of the refractive index and/or thermal expansion coefficients [which is the case for KBr (Sahagian and Pitha, 1971b) , the thermal and stress effects will tend to cancel. Interferometrically, then, the sample will appear to have a smaller absorption coefficient. Therefore, care must be taken to minimize thermal stresses during CO_2 laser heating if an accurate measure of the absorption coefficient is to be obtained by this technique.

3.2.2 DEVICE EVALUATION

Although the absorption coefficient is an important physical property influencing the performance of the laser window as a device, it is only one of approximately nine material parameters which contribute to thermal lensing phenomena in solids. A measure of this thermal distortion effect is the key requirement in predicting the optical performance of a material as a high-power laser window device. It has been shown (Hordvik, 1971) that attempts to obtain a device figure-of-merit based on measurements of thermally induced focal lengths meet with severe experimental difficulties. These limitations arise because of the low accuracy with which induced focussing can be measured for a diffraction limited beam.

Interferometry has traditionally been a powerful tool for testing the perfection of optical components. In particular, interferometric measurements are a highly accurate means of determining variations in optical path length. Since thermally induced, non-uniform path length changes are responsible for thermal lensing, interferometry may provide a sensitive and rapid indication of laser beam distortion. The approach, then, is to measure the effect of the beam on the window rather than the effect of the window on the beam.

Figure 13 shows a sequence of Twyman-Green interferometric patterns of a KBr sample with an incident CO_2 laser beam power density of 900 W/cm^2. The fringe patterns were produced by a He-Ne probe beam with the apparatus shown in Figure 11. Localized distortion of the pattern when the CO_2 laser radiation is incident on the window is clearly evident in Figure 13(b) and 13(c). The fringe pattern is seen to recover when exposure to the CO_2 laser beam terminated

TWYMAN-GREEN INTERFEROMETRIC MEASUREMENT OF KBr
50W CO_2 LASER, 900 W/cm^2, He-Ne PROBE BEAM

(a) Sample, No Beam

(b) 15 sec Exposure

Reproduced from best available copy.

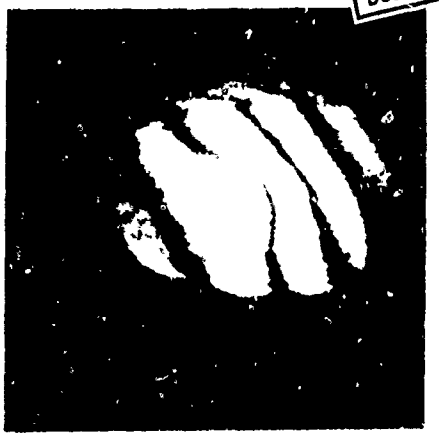

(c) 25 sec Exposure

(d) 2 sec After Exposure Termination

Figure 13. Time Dependence of Twyman-Green Interference Patterns of a KBr Window With 900 W/cm^2 Incident CO_2 Radiation

[Figure 13(d)]. Although window distortion is clearly evident from the interference patterns, attempts to accurately measure transmitted CO_2 beam intensity degradation were unsuccessful.

Measurements such as path length changes (that is, fringe movement) per unit time as a function of beamwidth or intensity may provide a rapid method of rating window materials.

In summary, interferometric techniques can be devised to measure absorption coefficients as well as thermal expansion coefficients, thermal coefficients of refractive index, and stress-optic effects. In addition to measuring material properties, interferometry may well provide rapid figure-of-merit ratings on the thermal lensing characteristics of high-power infrared laser windows.

4. SUMMARY

We have presented an overview of the principal elements of the current optical evaluation program for high-power laser windows at AFCRL. Various other aspects of the program were reported by Sahagian and Pitha (1971a). A Kirchoff vector diffraction theory of thermal lensing has led to predictions of materials best suited optically for use as laser windows. Calorimetric measurements of absorption coefficients of state-of-the-art window materials have been presented. The effects of surface preparation, sample inhomogeneities and imperfections, and scattering on calorimetric measurements have been discussed. Finally we have presented an interferometric method for measuring absorption coefficients and discussed window performance evaluation based on temporal shift of the interference pattern. As materials improve methods of optical evaluation must become more sensitive and it is anticipated that interferometry will find greater application in predicting the performance of laser windows.

Preceding page blank

Acknowledgments

The authors thank Dr. F. Harrigan of Raytheon Corp. and P. D. Gianino and A. Kahan for valuable discussions, Dr. A. Armington for the growth of many of the crystals used in this study, and P. Ligor and O. M. Clark for their able technical assistance.

Preceding page blank

References

Bendow, B. and Gianino, P.D. (1972) The On-Axis Distribution in Thermal Lensing in Solids, AFCRL Technical Report AFCRL 72-0322.

Bendow, B., Jasperse, J.R., and Gianino, P.D. (1971-72) AFCRL LQ-10 Quarterly Progress Reports Nos. 1-5.

Born, M., and Wolf, E. (1964) Principles of Optics, 2nd Edition, Macmillan Co.

Foster, J.D. and Osterink, L.M. (1968) Appl. Optics 7:2428.

Hordvik, A. (1971) in Conference on High Power Infrared Laser Window Materials, C. S. Sahagian and C.A. Pitha, Eds., AFCRL-71-0592, p. 389.

Horrigan, F.A., and Deutsch, T.F. (1971) Research in Optical Materials and Structures for High-Power Lasers, Final Technical Report, on ARPA Contract No. DAAH01-70-C-1251.

Jackson, J.D. (1962) Classical Electrodynamics, J. Wiley and Sons, N.Y.

Jasperse, J.R. and Gianino, P.D. (1972) J. Appl. Phys. 43, 1686.

Sahagian, C.S. and Pitha, C.A., Eds. (1971a) Proceedings of Conference on High-Power Infrared Laser Window Materials, AFCRL Special Reports No. 127, AFCRL-71-0592.

Sahagian, C.S. and Pitha, C.A., Eds. (1971b) Proceedings of Conference on High-Power Infrared Laser Window Materials, AFCRL Special Reports No. 127, AFCRL-71-0592, p. 155.

Sparks, M. (1971) J. Appl. Phys. 42:5029.